A new climate index controlling winter wave activity along the Atlantic coast of Europe: the West Europe Pressure Anomaly

Bruno Castelle [1,2], Guillaume Dodet [3], Gerd Masselink [4], Tim Scott [4]

[1]CNRS, UMR EPOC, France

[2]Univ. Bordeaux, UMR EPOC, France

[3]LETG-Brest Geomer UMR 6554 CNRS, Institut Universitaire Europeen de la Mer (UBO), Plouzane, France

[4]Coastal Processes Research Group, School of Biological and Marine Sciences, Plymouth University, UK

Key Points:

- A method is developed to objectively define an optimal climate index explaining winter wave activity variability along the W coast of Europe
- WEPA index is computed as the normalized difference in sea-level pressure measured between Ireland and Canary Islands
- WEPA significantly outscores other leading atmospheric modes in explaining the winter wave variability along most of the W coast of Europe

Corresponding author: Bruno Castelle, b.castelle@epoc.u-bordeaux1.fr

Abstract

A pioneering and replicable method based on a 66-year numerical weather and wave hindcast is developed to optimize a climate index based on the sea-level pressure that best explains winter wave height variability along the coast of W Europe, from Portugal to UK (36-52°N). The resulting so-called Western Europe Pressure Anomaly (WEPA) is based on the SLP gradient between the stations Valentia (Ireland) and Santa Cruz de Tenerife (Canary Islands). The WEPA positive phase reflects an intensified and southward-shifted SLP difference between the Icelandic low and the Azores high, driving severe storms that funnel high-energy waves towards western Europe southwards of 52°N. WEPA outscores by 25-150% the other leading atmospheric modes in explaining winter-averaged significant wave height, and even by a largest amount the winter-averaged extreme wave heights. WEPA is also the only index capturing the 2013/2014 extreme winter that caused widespread coastal erosion and flooding in western Europe.

1 Introduction

Large-scale patterns of atmospheric and oceanic variability on interannual and longer timescales, which are usually characterized in terms of oscillation around the mean, can be explained by teleconnections at the global scale [e.g. *McPhaden et al.*, 2006]. This variability has a profound influence on temperature, rainfall or storm tracks and intensity, and, in turn, on the terrestrial and marine biosphere [*Wang and Schimel*, 2003; *Bastos et al.*, 2016]. Coastal hazards are also strongly affected by large-scale climate patterns [e.g. *Goodwin et al.*, 2016]. *Barnard et al.* [2015] show that the El Nino/Southern Oscillation (ENSO) can cause extreme coastal erosion and flooding across the Pacific, with these changes in extreme wave climate having the potential to cause dramatic change in the equilibrium state of beaches [*Masselink et al.*, 2016a]. Therefore, winter and extreme coastal wave climate variability is a recent and important topic in climate studies [*Izaguirre et al.*, 2010] and it becomes increasingly important to link extreme wave energy arriving locally at the coast to large-scale oceanic and atmospheric variability [e.g. *Camus et al.*, 2014a; *Perez et al.*, 2014].

The North Atlantic Oscillation (NAO) has long been known to affect climate variability in the northern Hemisphere [*Hurrell*, 1995] and, as a result, the wave climate arriving at the west coast of Europe [e.g. *Bacon and Carter*, 1993; *Dodet et al.*, 2010; *Martinez-Asensio et al.*, 2016]. The influence of the NAO on waves along the Atlantic coast of Eu-

rope is particularly strong in the winter months [e.g. *Bromirski and Cayan*, 2015], when storm events are critical to both short- and long-term coastal behavior [e.g. *Stive et al.*, 2002]. A number of studies investigated how the NAO impacts shoreline change and coastal behavior, e.g. in UK [*Masselink et al.*, 2014] and France [*Robinet et al.*, 2016], showing that the NAO can explain a small, but significant, amount of the observed coastal variability. An explanation for this is that, while the NAO has a major impact on the Atlantic winter wave height in the northern sector (NW of the British islands), its influence is more subtle at more southern latitudes [UK, France, Spain and Portugal, *Dupuis et al.*, 2006]. In these regions, winter waves are more affected by other leading atmospheric modes in the N Atlantic, namely the East Atlantic (EA) and Scandinavia (SCAND) patterns [*Shimura et al.*, 2013]. The absence of a climate index specific to the Atlantic coast of Europe and the resulting lack of understanding of the major atmospheric control on winter wave climate along this coast is a major drawback. A striking example is the winter 2013/2014 that was characterized by extreme winter wave activity [*Masselink et al.*, 2016a] and sea level events [*Haigh et al.*, 2016] along the Atlantic coast of Europe, with the largest winter-averaged wave energy arriving at the coast in mid to southern latitude, i.e. 55°N - 38°N, over at least the last 67 years. This 2013/2014 winter, which caused unprecedented coastal erosion in many locations from western Europe down to Morocco [e.g. *Castelle et al.*, 2015; *Suanez et al.*, 2015; *Masselink et al.*, 2016a,b], was not captured by any of the above-mentioned climate indices. From the perspective of coastal hazards, climate indices are therefore also relevant if they can explain extreme wave energy events, which are critical to flooding, cliff failure and beach erosion [e.g. *Menendez et al.*, 2008; *Ruggiero et al.*, 2010; *Barnard et al.*, 2011].

Climate indices can be computed through the principal empirical orthogonal function (EOF) of surface pressure derived from numerical weather hindcast to give a physically-based expression of atmospheric structure [e.g. *Rogers*, 1981]. Alternatively, indices based on sea-level pressure (SLP) measurements can also be computed based on well-known atmospheric structures if relevant land-based measurements exist. For instance, the NAO index was first computed using measured SLP difference between Iceland and a southern station (Lisbon, Azores or Gibraltar) to capture the variability between the Azores high and the Icelandic low [*Hurrell*, 1995]. EOF- and SLP-based NAO indices generally show very good agreement [*Hurrell and Deser*, 2009]. However, compared to EOF-based indices that need reliable numerical hindcast of large-scale SLP patterns, SLP-based

indices using 2 SLP stations have the advantage that they can be calculated back to the early 1900s, or even 1800s, as measured weather data from more than 100 years are not uncommon across the world [*Trenberth and Paolino*, 1980; *Jones et al.*, 2013; *Goodwin*, 2005].

In this paper, we develop a new SLP-based climate index that acts as a primary control on winter waves along the Atlantic coast of Europe. Previous studies systematically developed or used climate indices based on their atmospheric expression to further address their influences on, for instance, rainfall, temperature or wave climate. Instead, here the index is reverse engineered from the end product, namely winter wave height along the west coast of Europe, as large wave heights are the primary cause of coastal hazards. The optimal SLP gradient that best explains the observed variability of winter wave activity is objectively searched from a 66-year numerical weather and wave hindcast. It will be shown that our new index explains between 40% and 90% of the observed winter-averaged wave height variability from southern Ireland down to Portugal, where all the other indices explain at best 40%, and that it also captures the variability of extreme wave heights. The positive phase of this climate index reflects an intensified latitudinal SLP gradient in the NE Atlantic, between Ireland and Canary Islands, driving increased W-SW winds around 45°N that funnel high-energy waves towards western Europe together with deep low pressure systems passing over the UK.

2 Data and method

2.1 Atmospheric data and climate indices

We used the 6-hourly SLP and 10-m wind ($\vec{u}_{10}$) fields (2.5°x2.5°) of the NCEP/NCAR reanalysis project from January 1948 to April 2016 [*Kalnay et al.*, 1996]. Storm tracks were computed using the algorithm described in *Murray and Simmonds* [1991]. This method is based on the local maxima in relative vorticity, rather than local pressure minima, as the former was shown to also identify small-scale pressure systems, and was further validated in the N Atlantic Ocean [*Pinto et al.*, 2005]. Monthly teleconnection indices, based on the rotated EOF analysis described in *Barnston and Livezey* [1987] and available since January 1950, were downloaded from the National Oceanic and Atmospheric Administration (NOAA) Climate Prediction Center (www.cpc.ncep.noaa.gov). We used the climate indices associated with the leading atmospheric modes in the N Atlantic and with proven links

with the wave climate in the NE Atlantic [*Shimura et al.*, 2013], namely EOF-based NAO, EA and SCAND.

2.2 Wave modelling

To address long-term wave height variability in the N Atlantic, we used the same approach as detailed in *Masselink et al.* [2016a], extending the modeling effort to span the 68-year period 1948-2016. The spectral wave model Wave Watch III V14.18 [*Tolman*, 2014] was implemented on a 0.5° resolution grid covering the N Atlantic Ocean (80°-0°W; 0°-70°N) forced with the 6-hourly wind fields $\vec{u}_{10}$ described in Section 2.1. For more detail on the modelling approach and the validation against a wealth of buoys along the European shelf, please see *Masselink et al.* [2016a]. Six virtual wave buoys were used to address the spatial distribution of wave heights along the entire Atlantic coast of Europe from Scotland in the North to Portugal in the South (Figure 1c): SC: Scotland; IR: Ireland; BR: Brittany; BI: Biscay; GA: Galicia; PT: Portugal.

2.3 Methodology

Winter averages of climate indices, grid point significant wave height H_s and their 90%, 95% and 99% exceedance values ($H_{s90\%}$, $H_{s95\%}$ and $H_{s90\%}$), $\vec{u}_{10}$ and SLP was computed by averaging the monthly values for the Boreal winter [December, January, February and March - DJFM, consistent with earlier climate studies, e.g. *Camus et al.*, 2014b; *Martinez-Asensio et al.*, 2016; *Ouzeau et al.*, 2011] from 1950 to 2016 (66 winters). The relationship between winter-averaged H_s and all possible virtual climate indices was studied computing the correlation coefficient R between the normalized time series of winter-averaged H_s and the difference of normalized SLP between all possible grid point pairs within the whole domain (80°-0°W; 0°-70°N). For each virtual buoy along the Atlantic coast of Europe (Figure 1c), the pair of virtual SLP stations that gave the highest correlation R was used to define the optimal climate index to explain the variability of winter-averaged H_s at that location. The same approach was also applied for only grid point pairs containing land within a corresponding 2.5°x2.5° cell to further search for existing, relevant, long-term SLP measurements.

3 Results and discussion

Figure 1a displays the optimal winter-averaged SLP gradients obtained by searching for virtual stations anywhere within the domain. It is of interest to note that for SC and IR, the south virtual SLP station of the optimal latitudinal gradient is closer to the Iberian Peninsula than to the Azores, suggesting that correlations between NAO and winter-averaged H_s for northern latitudes should be higher when using the Lisbon/Gibraltar - Reykjavik NAO SLP-station-based index than when using the Ponta-Delgada (Azores) - Reykjavik NAO SLP-station-based index. The corresponding correlation coefficient R is high (Table 1, 0.95 and 0.93 for SC and IR, respectively), meaning that the optimal NAO-like index explains more than 86% of the winter-averaged H_s variability off Scotland and Ireland. This is consistent with earlier studies [e.g. *Dodet et al.*, 2010; *Bertin et al.*, 2013; *Bromirski and Cayan*, 2015; *Martinez-Asensio et al.*, 2016] showing that the NAO has a major impact on the winter-averaged H_s along the northern coast of Europe (NW of British isles). Going southward, the optimal SLP gradients become increasingly both longitudinal and/or shifted southward, still with high correlation ($R > 0.89$, Table 1). While all the 4 southern buoys correlate with SLP gradients based on a northern virtual station within or in the vicinity of Ireland, the southern virtual stations are systematically located in the open ocean, inhibiting the use of land-based SLP pair measurements.

Figure 1b is based on the same analysis, but using land-based stations only. The largest amount of winter-averaged H_s variability at the Scottish buoy (SC) is explained by the SLP-based Iceland - Lisbon definition of the NAO, which shows slightly better correlation than using the Iceland - Gibraltar definition. In contrast, the largest amount of winter-averaged H_s variability at all the other buoys (except PT) is explained by the anomaly in SLP gradients between Ireland and various southern locations (Azores, Canary Islands, Spain or France), with systematically $R > 0.89$ (Table 1). Of note, while Figure 1b displays the optimal land-based SLP gradients, some other SLP gradients also show very good skill. For instance, the optimal SLP gradient for the BI (Bay of Biscay) buoy is Ireland - Azores ($R = 0.92$), but the SLP gradient Ireland - Canary Islands also shows very good skill ($R = 0.86$). Similarly, the NAO (Iceland - Lisbon gradient definition) shows very good skill ($R = 0.79$) for the IR buoy, although it is outscored by a SLP gradient between Ireland and Brittany ($R = 0.9$, see Figure 1b and Table 1).

It is relevant to look for a climate index that skillfully explains the winter-averaged H_s along the entire Atlantic coast of Europe. However, the atmospheric patterns controlling wave heights at the southern and northern latitudes of the west coast of Europe are significantly different and the NAO is known to strongly control winter height the northern regions. Therefore, it is relevant to address the region where the NAO and other climate indices show poor skill, i.e., from S Ireland to S Portugal. Accordingly, we searched for the optimal SLP gradient that, on average, shows the best correlation with the 4 southern buoys (black line gradient in Figure 1a, b).

Results show that the variability of winter-averaged H_s is strongly controlled by an optimal SLP gradient that is essentially both latitudinal and longitudinal with a northern station in Ireland (Figure 1a). In contrast, the optimal gradient using land-based stations only is essentially latitudinal between Ireland and Canary Islands (Figure 1b), meaning that the loss of longitudinal SLP gradient is the result of the need to have land-based stations. It is important to note that the optimal land-based SLP gradient showing the best correlation averaged over the 6 buoys is also Ireland - Canary Islands, although poor correlation is found at the northern latitudes (see below). Hereafter, this optimal climate index is referred to as the Western Europe Pressure Anomaly (WEPA) and is calculated from the daily measured SLP at Valentia station (Ireland) and Santa Cruz de Tenerife, Canary Island (Spain). The winter time series of WEPA is provided as supplementary material.

Figure 2 shows the spatial distribution of the correlation between the winter-averaged H_s as well as the winter-averaged $H_{95\%}$, and 3 climate indices, namely NAO, EA and our new index WEPA. The spatial distribution for SCAND is not shown here as poor correlation is found across the whole E Atlantic. In line with earlier studies [e.g. *Dodet et al.*, 2010; *Shimura et al.*, 2013; *Bromirski and Cayan*, 2015], the NAO is found to have a strong influence on the winter-averaged H_s at the northern latitudes (Figure 2a, c; R = 0.89 for the SC buoy in Table 1). This influence dramatically decreases south of 52°N (e.g. R = 0.45 at BI station, Figure 2a, c). In contrast, the EA shows better correlation south of 52°N, although the correlation R along the coast is systematically below 0.65 (see Table 1 and Figure 2d, f), meaning that EA explains at best approximately 40% of the observed winter-averaged H_s variability. Figure 2g, i shows the same analysis for our new climate index WEPA. Clearly, the correlation with winter-averaged H_s across the Atlantic coast of Europe south of 52°N is greatly increased ($R > 0.8$), with even areas show-

ing $R > 0.9$-0.95 (e.g. $R = 0.91$ at Galicia buoy GA, Table 1). In addition, only WEPA captures the 2013/2014 winter that was characterized by extreme wave activity along the Atlantic coast of Europe [*Masselink et al.*, 2016a, Figure 2i]. This is further emphasized by the spatial distribution of the correlation between the winter-averaged $H_{s95\%}$ and the same three climate indices (Fig. 2b, e and h). Correlation patterns for winter-averaged $H_{s95\%}$ are very similar to those of winter-averaged H_s, showing that WEPA captures both the temporal (2013/2014 winter, Fig. 2i) and spatial (Fig. 2h) variability of extreme wave energy.

The relevance of the WEPA for the W coast of Europe is further emphasized in Figure 3 that displays the spatial distribution of the optimal climate indices to explain the winter wave climate within the NE Atlantic. The optimal climate index is defined as the index with the highest R^2 associated with the local winter-averaged H_s. Here, we now switch from R to R^2 both to address the amount of variability explained by the index and to account for negative correlations. Disregarding the WEPA the two optimal climate indices explaining winter-averaged H_s along the Atlantic coast of Europe north and south of 52°N are clearly NAO and EA, respectively (Figure 3a). This corroborates the results of *Shimura et al.* [2013] who included 9 teleconnection index in their study. Including the WEPA, Figure 3b shows that WEPA largely outscores the other indices along the Atlantic coast of Europe south of 52°N. Compared to EA, WEPA increases the explanation of the winter-averaged H_s variability by 25-150% (see the large increase in R^2 in Figure 3c). This improvement is even better when considering extreme wave events Figure 3d-f) with, for instance, an increase for $H_{s99\%}$ exceeding 200% along most of the Spanish and Portuguese coasts (Figure 3f).

To further understand the control of WEPA on winter wave climate along the Atlantic coast of Europe, Figure 4 provides physical insight into the atmospheric phenomenon for both the NAO and the WEPA, with positive and negative phase of each index addressed by averaging the 5 years with the largest and smallest values, respectively (Figure 4g). During the positive phase of the NAO (NAO+, Figure 4a-d), larger and smaller waves are observed at northern and southern latitudes, respectively (Figure 4a, b). The strengthened latitudinal SLP gradient, which corresponds to a wider and stronger anticyclone centered on the Azores and lower pressures in high latitudes (Figure 4c, d), drives deep low pressure systems passing between Greenland and Scotland (Figure 4e) associated with increased W-SW winds around 60°N (Figure 4d). This drives larger winter waves at

northern latitudes during NAO+. The opposite situation is observed during the negative phase of the NAO (NAO-, Figure 4f-j) with fewer and less deep, southward-shifted, low pressure systems driving slightly larger and much smaller winter waves in the southern and northern latitudes, respectively. During the positive phase of the WEPA, larger waves are observed from the mid to southern latitudes with a maximum increase in the Bay of Biscay (Figure 4k, l). The SLP pattern consists of a latitudinal dipole of anomaly that resembles a 15° southward-shifted NOA pattern, driving increased W-SW winds around 45°N funneling towards western Europe (Figure 4m, n). This SLP anomaly pattern also drives a large number of deep low pressure systems passing over Ireland and UK (Figure 4t) together with much stronger than average SW to W winds across the middle latitudes (Figure 4n). This generates larger waves across the Atlantic coast of Europe south of 52°N during WEPA+. In contrast, during the negative phase of WEPA, which resembles a northward-shifted and less intense NOA+ pattern, fewer storms and smaller winter waves are observed from SW Ireland to S Portugal.

Both phases of the WEPA are associated with profound large-scale changes in mean SLP and wind patterns and, as a result, in the intensity, location and trajectories of severe storm tracks driving extreme wave events. Although the WEPA can be interpreted as a southward shifted NAO, the indices WEPA and NAO are not correlated (R = 0.08). The key factor determining this optimal SLP gradient is the reduction in the northerly extent of SLP gradients by replacing Iceland by Ireland as the northern SLP station. Other SLP-based indices were computed based on Valentia station (Ireland) to the north and other southern stations (e.g. Azores, Gibraltar). These indices also show excellent, although slightly inferior, overall skill from SW Ireland to S Portugal. These indices also outscore WEPA at some locations. For instance, the SLP-based index between Ireland and Azores shows outstanding skill in the Bay of Biscay, explaining 85% of the observed winter-averaged H_s at the BI buoy, but does a poor job in S Portugal. Similarly to WEPA, the EA pattern is often interpreted as a southward-shifted NAO pattern. However, despite 36% of the WEPA variability being explained by EA, the two indices show different skill. For instance, only the WEPA captures the extreme winter 2013/2014 [*Masselink et al.*, 2016a]. In addition, WEPA is much more relevant than EA along the coast of Europe, while EA shows more skill further offshore eastward of -25°. WEPA is therefore of much more relevance than EA from the coastal hazards perspective, which is further emphasized in the analysis of $H_{s90\%}$, $H_{s95\%}$ and $H_{s99\%}$ (Figure 3d-f). Finally, as the Valentia and Canary Is-

land SLP data have been measured from 1943 a 74-year time series of the WEPA index is available (supplementary material) to further explore its influence on wave climate in the N Atlantic, particularly in the coastal regions. In addition, potential relationships between WEPA and, for instance, rainfall and temperatures in western Europe should be explored.

4 Conclusions

A generic method using numerical weather and wave hindcast was developed to identify the optimal SLP-based climate index explaining winter wave activity along the Atlantic coast of Europe spanning 1950-2016. The resulting so-called Western Europe Anomaly (WEPA) index is based on the normalized SLP difference measured between the stations Valentia (Ireland) and Santa Cruz de Tenerife (Canary Islands, Spain). The positive phase of WEPA reflects intensified latitudinal SLP gradient in the NE Atlantic that drives increased W-SW winds around 45° associated with severe storms, many eventually passing over UK, which funnel high-energy waves towards western Europe. Complementary to the NAO that controls winter-averaged H_s in the NW of the British Island (> 52°N), our new index WEPA explains between 40% and 90% of the observed winter-averaged H_s variability along the Atlantic coast of Europe southward of 52°. WEPA largely outscores the SCAND and EA indices, which are often argued as the primary control of winter wave activity in this region. WEPA is also the most relevant index to capture extreme wave height both spatially and temporally, like for the extreme 2013/2014 that caused severe erosion along the Atlantic coast of Europe. We therefore anticipate that the WEPA index is critical to understand coastal hazards in western Europe. Finally, further testing in other coastal regions worldwide and for other end products (e.g. rainfall) should be carried out to assess the generality of this method to develop improved climate indices.

Acknowledgments

This work was financially supported by the *Agence Nationale de la Recherche* (ANR) through the project CHIPO (ANR-14-ASTR-0004-01) and the "Laboratoire d'Excellence" LabexMER (ANR-10-LABX-19-01) program, and by the AST "Evenements extremes" of the *Observatoire Aquitain des Sciences de l'Univers* (OASU). GD was funded by the research program PROTEVS (12CR6) conducted by the French Naval Oceanographic and Hydrographic Department (SHOM). GM and TS were funded by the NERC BLUE-coast project (NE/N015525/1). We acknowledge the SLP data providers in the ECA&D

300 project [http://www.ecad.eu, *Klein Tank et al.*, 2002] and the Irish Meteorological Ser-
301 vice (http://www.met.ie/climate-request/) for the Valentia Observatory data, the develop-
302 ers of the WAVEWATCH III TM model and the NCEP Reanalysis data provided by the
303 NOAA/OAR/ESRL PSD. The winter time series of WEPA is provided as supplementary
304 material of this paper. WW3 outputs can be provided on demand to GD (guillaume.dodet@univ-
305 brest.fr).

306 References

307 Bacon, S., and D. J. T. Carter (1993), A connection between mean wave height and at-
308 mospheric pressure gradient in the north atlantic, *International Journal of Climatology*,
309 *13*(4), 423–436, doi:10.1002/joc.3370130406.

310 Barnard, P., A. Short, M. Harley, K. Splinter, S. Vitousek, I. Turner, J. Allan, M. Banno,
311 K. Bryan, A. Doria, J. Hansen, S. Kato, Y. Kuriyama, E. Randall-Goodwin, P. Rug-
312 giero, I. Walker, and D. Heathfield (2015), Coastal vulnerability across the Pacific
313 dominated by El Nino/Southern Oscillation, *Nature Geoscience*, *8*(10), 801–807, doi:
314 10.1038/ngeo2539.

315 Barnard, P. L., J. Allan, J. E. Hansen, G. M. Kaminsky, P. Ruggiero, and A. Doria (2011),
316 The impact of the 2009âĂŞ10 el niÃśo modoki on u.s. west coast beaches, *Geophysical*
317 *Research Letters*, *38*(13), doi:10.1029/2011GL047707, l13604.

318 Barnston, A. G., and R. E. Livezey (1987), Classification, Seasonality and Persistence of
319 Low-Frequency Atmospheric Circulation Patterns, *Monthly Weather Review*, *115*(6),
320 1083–1126.

321 Bastos, A., I. Janssens, C. Gouveia, R. Trigo, P. Ciais, F. Chevallier, J. Penuelas, C. Ro-
322 denbeck, S. Piao, P. Friedlingstein, and S. Running (2016), European land CO2 sink
323 influenced by NAO and East-Atlantic Pattern coupling, *Nature Communications*, *7*, doi:
324 10.1038/ncomms10315.

325 Bertin, X., E. Prouteau, and C. Letetrel (2013), A significant increase in wave height in
326 the North Atlantic Ocean over the 20th century, *Global and Planetary Change*, *106*, 77–
327 83.

328 Bromirski, P. D., and D. R. Cayan (2015), Wave power variability and trends across the
329 North Atlantic influenced by decadal climate patterns, *Journal of Geophysical Research:*
330 *Oceans*, *120*(5), 3419–3443, doi:10.1002/2014JC010440.

Camus, P., F. J. Mendez, I. J. Losada, M. Menendez, A. Espejo, J. Perez, A. Rueda, and Y. Guanche (2014a), A method for finding the optimal predictor indices for local wave climate conditions, *Ocean Dynamics*, *64*(7), 1025–1038, doi:10.1007/s10236-014-0737-2.

Camus, P., M. Menendez, F. J. Mendez, C. Izaguirre, A. Espejo, V. Canovas, J. Perez, A. Rueda, I. J. Losada, and R. Medina (2014b), A weather-type statistical downscaling framework for ocean wave climate, *Journal of Geophysical Research: Oceans*, *119*(11), 7389–7405, doi:10.1002/2014JC010141.

Castelle, B., V. Marieu, S. Bujan, K. D. Splinter, A. Robinet, N. Senechal, and S. Ferreira (2015), Impact of the winter 2013-2014 series of severe Western Europe storms on a double-barred sandy coast: Beach and dune erosion and megacusp embayments, *Geomorphology*, *238*, 135–148.

Dodet, G., X. Bertin, and R. Taborda (2010), Wave climate variability in the north-east atlantic ocean over the last six decades, *Ocean Modelling*, *31*(3-4), 120 – 131.

Dupuis, H., D. Michel, and A. Sottolichio (2006), Wave climate evolution in the bay of biscay over two decades, *Journal of Marine Systems*, *63*(3 - 4), 105 – 114.

Goodwin, I. D. (2005), A mid-shelf wave direction climatology for south-eastern Australia, and its relationship to the El Nino - Southern Oscillation, since 1877 AD, *International Journal of Climatology*, *25*, 1715 – 1729.

Goodwin, I. D., T. R. Mortlock, and S. Browning (2016), Tropical and extratropical-origin storm wave types and their influence on the east australian longshore sand transport system under a changing climate, *Journal of Geophysical Research: Oceans*, *121*(7), 4833–4853, doi:10.1002/2016JC011769.

Haigh, I. D., M. P. Wadey, T. Wahl, O. Ozsoy, R. J. Nicholls, J. M. Brown, K. Horsburgh, and B. Gouldby (2016), Spatial and temporal analysis of extreme sea level and storm surge events around the coastline of the UK, *Sci. Data*, *3:160107*, doi:10.1038/sdata.2016.107.

Hurrell, J. W. (1995), Decadal Trends in the North Atlantic Oscillation: Regional Temperatures and Precipitation, *Science*, *269*(5224), 676–679, doi:10.1126/science.269.5224.676.

Hurrell, J. W., and C. Deser (2009), North Atlantic climate variability: The role of the North Atlantic Oscillation , *Journal of Marine Systems*, *78*(1), 28 – 41.

Izaguirre, C., F. J. Mendez, M. Menedez, A. Luceno, and I. J. Losada (2010), Extreme wave climate variability in Southern Europe using satellite data, *Journal of Geophysical Research*, *C04009*, doi::10.1029/2009JC005802.

Jones, P. D., T. J. Osborn, and K. R. Briffa (2013), Pressure-based measures of the North Atlantic Oscillation (NAO), a comparison and an assessment of changes in the strength of the NAO and its influence on surface claimte parameters, in *The North Atlantic Oscillation: Climatic Significance and Environmental Impact*, edited by J. W. Hurrell, Y. Kushnir, G. Ottersen, and M.Visbeck, pp. 1–35, American Geophysical Union, doi: 10.1029/134GM01.

Kalnay, E., M. Kanamitsu, R. Kistler, W. Collins, D. Deaven, L. Gandin, M. Iredell, S. Saha, G. White, J. Woollen, Y. Zhu, A. Leetmaa, R. Reynolds, M. Chelliah, W. Ebisuzaki, W. Higgins, J. Janowiak, K. C. Mo, C. Ropelewski, J. Wang, R. Jenne, and D. Joseph (1996), The NCEP/NCAR 40-Year Reanalysis Project, *Bulletin of the American Meteorological Society*, *77*(3), 437–471.

Klein Tank, A. M. G., J. B. Wijngaard, G. P. Konnen, R. Bohm, G. DemarÃl'e, A. Gocheva, M. Mileta, S. Pashiardis, L. Hejkrlik, C. Kern-Hansen, R. Heino, P. Bessemoulin, G. Muller-Westermeier, M. Tzanakou, S. Szalai, T. Palsdottir, D. Fitzgerald, S. Rubin, M. Capaldo, M. Maugeri, A. Leitass, A. Bukantis, R. Aberfeld, A. F. V. van Engelen, E. Forland, M. Mietus, F. Coelho, C. Mares, V. Razuvaev, E. Nieplova, T. Cegnar, J. Antonio Lopez, B. Dahlstrom, A. Moberg, W. Kirchhofer, A. Ceylan, O. Pachaliuk, L. V. Alexander, and P. Petrovic (2002), Daily dataset of 20th-century surface air temperature and precipitation series for the European Climate Assessment, *International Journal of Climatology*, *22*(12), 1441–1453, doi:10.1002/joc.773.

Martinez-Asensio, A., M. N. Tsimplis, M. Marcos, X. Feng, D. Gomis, G. Jorda, and S. A. Josey (2016), Response of the North Atlantic wave climate to atmospheric modes of variability, *International Journal of Climatology*, *36*(3), 1210–1225, doi: 10.1002/joc.4415.

Masselink, G., M. Austin, T. Scott, T. Poate, and P. Russell (2014), Role of wave forcing, storms and NAO in outer bar dynamics on a high-energy, macro-tidal beach, *Geomorphology*, *226*, 76–93.

Masselink, G., B. Castelle, T. Scott, G. Dodet, S. Suanez, D. Jackson, and F. Floc'h (2016a), Extreme wave activity during 2013/2014 winter and morphological impacts along the Atlantic coast of Europe, *Geophysical Research Letters*, *43*(5), 2135–2143,

doi:10.1002/2015GL067492.

Masselink, G., T. Scott, T. Poate, P. Russell, M. Davidson, and D. Conley (2016b), The extreme 2013/2014 winter storms: hydrodynamic forcing and coastal response along the southwest coast of England, *Earth Surface Processes and Landforms*, *41*(3), 378–391, doi:10.1002/esp.3836.

McPhaden, M. J., S. E. Zebiak, and M. H. Glantz (2006), ENSO as an Integrating Concept in Earth Science, *Science*, *314*(5806), 1740–1745, doi:10.1126/science.1132588.

Menendez, M., F. J. Mendez, I. J. Losada, and N. E. Graham (2008), Variability of extreme wave heights in the northeast Pacific Ocean based on buoy measurements, *Geophysical Research Letters*, *35*(L22607).

Murray, R., and I. Simmonds (1991), A numerical scheme for tracking cyclone centres from digital data. Part I: development and operation of the scheme, *Australian Meteorological Magazine*, *39*(3), 155–166.

Ouzeau, G., J. Cattiaux, H. Douville, A. Ribes, and D. Saint-Martin (2011), European cold winter 2009-2010: How unusual in the instrumental record and how reproducible in the arpege-climat model?, *Geophysical Research Letters*, *38*(11), doi:10.1029/2011GL047667, l11706.

Perez, J., F. J. Mendez, M. Menendez, and I. J. Losada (2014), ESTELA: a method for evaluating the source and travel time of the wave energy reaching a local area, *Ocean Dynamics*, *64*(8), 1181–1191, doi:10.1007/s10236-014-0740-7.

Pinto, J. G., T. Spangehl, U. Ulbrich, and P. Speth (2005), Sensitivities of a cyclone detection and tracking algorithm: individual tracks and climatology, *Meteorologische Zeitschrift*, *14*(6), 823–838, doi:10.1127/0941-2948/2005/0068.

Robinet, A., B. Castelle, D. Idier, G. Le Cozannet, M. Déqué, and E. Charles (2016), Statistical modeling of interannual shoreline change driven by North Atlantic climate variability spanning 2000-2014 in the Bay of Biscay, *Geo-Marine Letters*, pp. 1 – 12, doi:10.1007/s00367-016-0460-8.

Rogers, J. C. (1981), Spatial Variability of Seasonal Sea Level Pressure and 500 mb Height Anomalies, *Monthly Weather Review*, *109*(10), 2093–2106.

Ruggiero, P., P. D. Komar, and J. C. Allan (2010), Increasing wave heights and extreme value projections: the wave climate of the US Pacific Northwest, *Coastal Engineering*, *57*, 539 – 552.

Shimura, T., N. Mori, and H. Mase (2013), Ocean Waves and Teleconnection Patterns in the Northern Hemisphere, *Journal of Climate*, *26*(21), 8654–8670, doi:10.1175/JCLI-D-12-00397.1.

Stive, M. J. F., S. G. J. Aarninkhof, L. Hamm, H. Hanson, M. Larson, K. M. Wijnberg, R. J. Nicholls, and M. Capobianco (2002), Variability of shore and shoreline evolution, *Coastal Engineering*, *47*, 211–235.

Suanez, S., R. Cancouet, F. Floc'h, E. Blaise, F. Ardhuin, J.-F. Filipot, J.-M. Cariolet, and C. Delacourt (2015), Observations and predictions of wave runup, extreme water levels, and medium-term dune erosion during storm conditions, *Journal of Marine Science and Engineering*, *3*(3), 674, doi:10.3390/jmse3030674.

Tolman, H. L. (2014), User manual and system documentation of WAVEWATCH III version 4.18, in *NOAA/NWS/NCEP/MMAB Technical Note 316*, p. 194pp.

Trenberth, K. E., and D. A. Paolino (1980), The Northern Hemisphere Sea-Level Pressure Data Set: Trends, Errors and Discontinuities, *Monthly Weather Review*, *108*(7), 855–872.

Wang, G., and D. Schimel (2003), Climate Change, Climate Modes, and Climate Impacts, *Annual Review of Environment and Resources*, *28*(1), 1–28, doi:10.1146/annurev.energy.28.050302.105444.

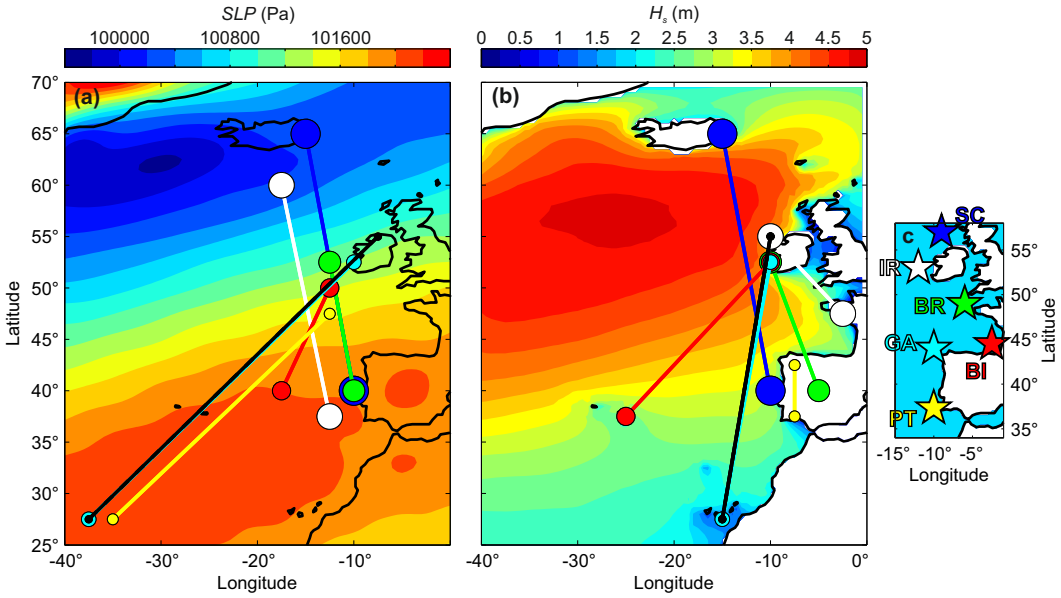

445 **Figure 1.** Simulated optimal winter-averaged (DJFM) SLP gradients from (a) virtual stations anywhere
446 within the domain (80°-0°W; 0°-70°N) and (b) virtual stations containing land within the corresponding
447 2.5°x2.5° cell, which explain the largest amount of variability of winter-averaged H_s at (c) 6 virtual wave
448 buoys along the W coast of Europe. SC: Scotland; IR: Ireland; BR: Brittany; BI: Biscay; GA: Galicia; PT:
449 Portugal. The buoys considered for each gradient are given by the color code, and the black gradient in (a,b)
450 indicates the optimal pressure gradient combining the 4 southern buoys BR, BI, GA and PT. The winter-
451 averaged (1950-2016) SLP and H_s are colored in the background in panel (a) and (b), respectively.

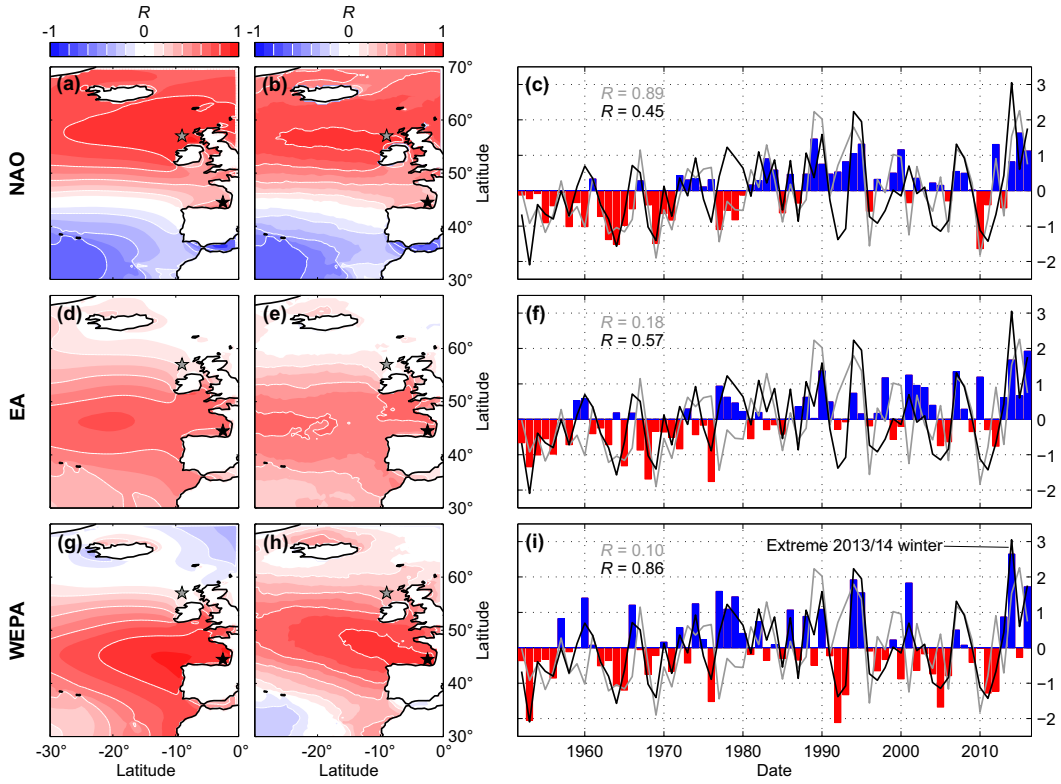

Figure 2. Left-hand and middle panels show the spatial correlation of the winter(DJFM)-averaged H_s and $H_{s95\%}$, respectively, against the winter-averaged (a,b) NAO and (d,e) EA indices, and against (g,h) our new WEPA index computed as the normalized SLP difference measured between station Valentia (Ireland) and station Santa Cruz de Tenerife (Canary Islands, Spain). Right-hand panels: time series of the corresponding indices with superimposed normalized winter-averaged H_s simulated at the buoys SC (Scotland, black) and BI (Biscay, grey) with corresponding correlation coefficient.

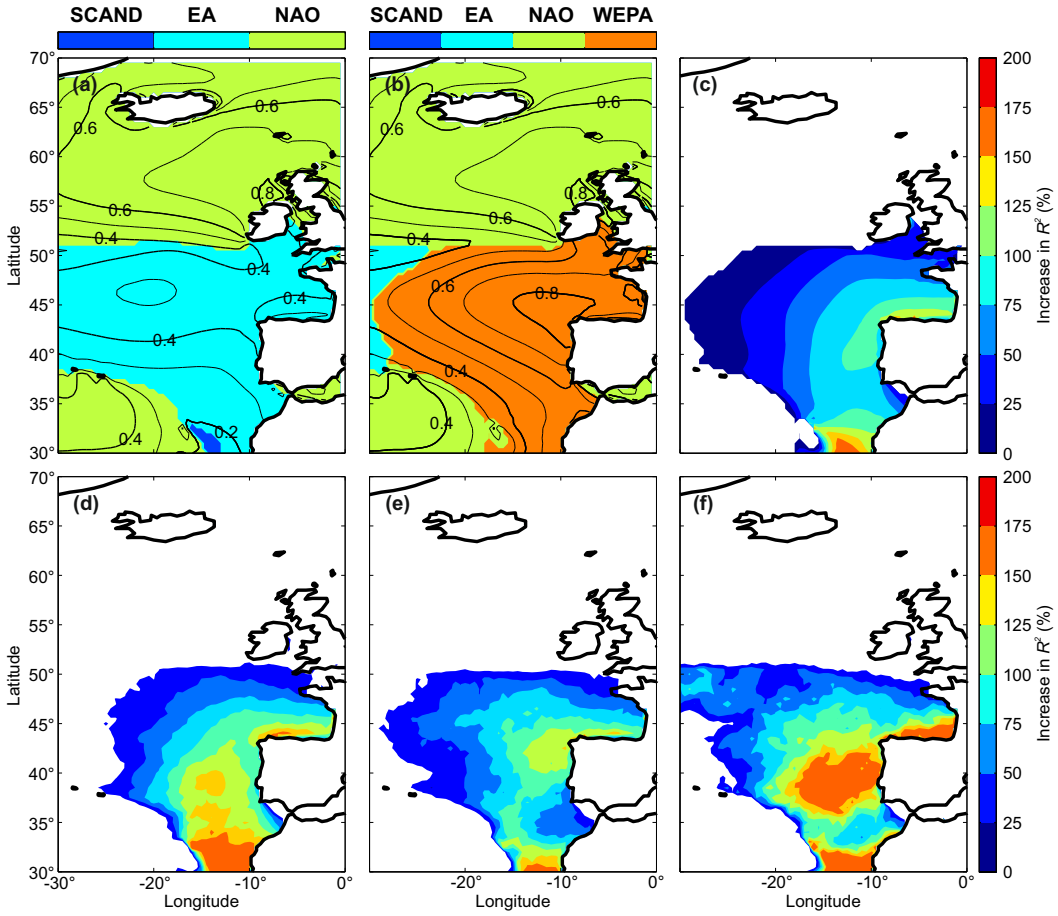

458 **Figure 3.** Top panels: spatial distribution of optimal climate indices explaining the largest variability of
459 local winter-averaged H_s (DJFM) (a) ignoring and (b) accounting for our new WEPA climate index com-
460 puted as the normalized SLP difference measured between station Valentia (Ireland) and station Santa Cruz
461 de Tenerife (Canary Islands, Spain), with the corresponding regression coefficient R^2 contoured in the back-
462 ground of both panels. (c) Corresponding spatial distribution of the increase (%) in R^2 including the WEPA
463 as a climate index in the NE Atlantic, in winter-averaged H_s predictability. WEPA index increases by 25 to
464 125% the explanation of the winter-averaged H_s variability along the Atlantic coast of Europe from S Ireland
465 to Portugal. Bottom panels show the same analysis as in (c) but for (d) $H_{s90\%}$, (e) $H_{s95\%}$ and (f) $H_{s99\%}$.

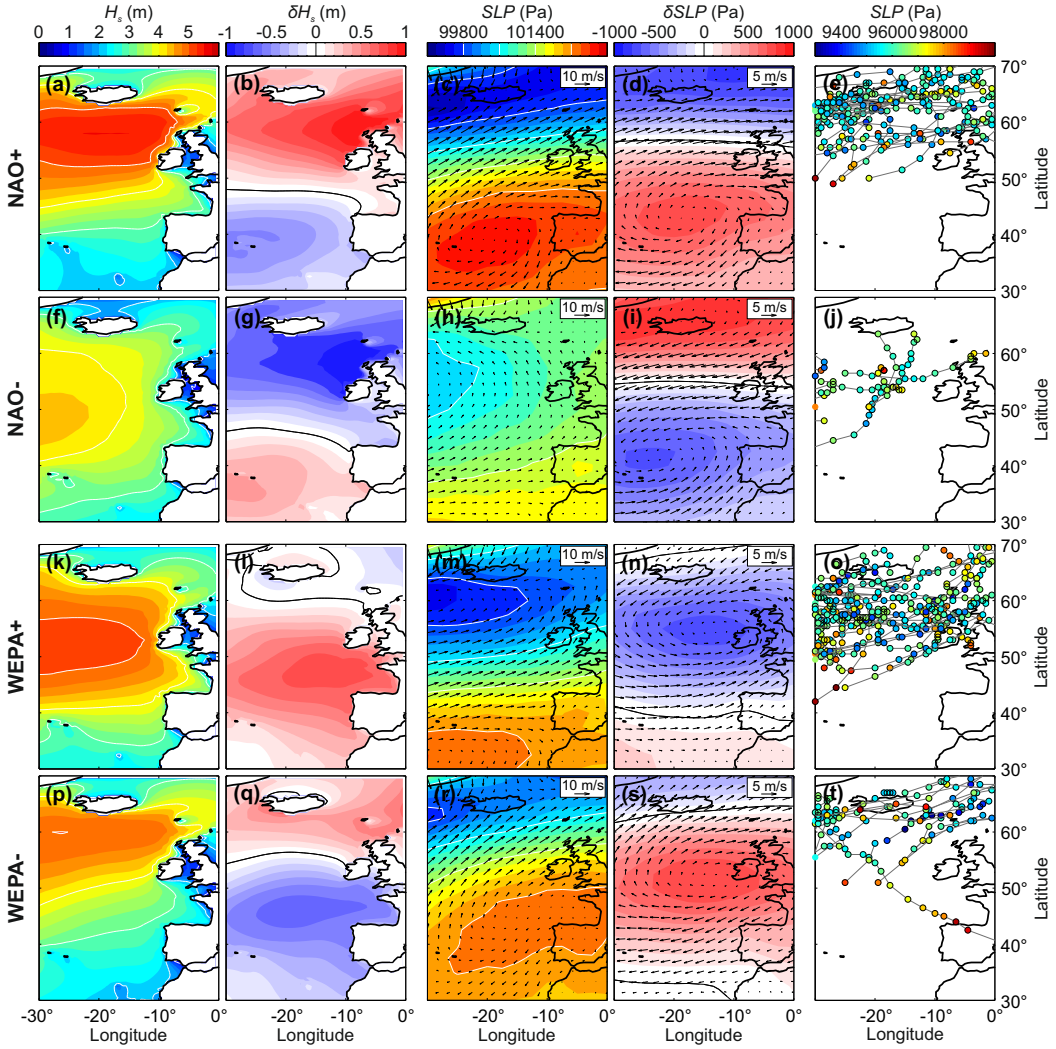

Figure 4. Influence of the NAO and WEPA indices on winter-averaged H_s, SLP, 10-m surface winds and storm tracks, with positive and negative phase of each index addressed by averaging the 5 years with the largest and smallest index values over 1950-2016, respectively. First column: winter-averaged H_s; second column: corresponding anomaly; third column: winter-averaged SLP with superimposed $\vec{u}_{10}$ field; fourth column: corresponding anomaly; fifth column: superimposed storm tracks over the 5 years with the colored circles indicating the sea-level pressure at the center of the low pressure system every 6 hours. Note that for clarity and to focus on the more severe storms, only identified storms that have a low pressure center deeper than 96 000 Pa are plotted. By order of decreasing importance, the 5 winter years considered for each index phase are: NAO+ (2015, 1989, 1995, 2012, 2000); NAO- (2010, 1964, 1969, 1963, 1977); WEPA+ (2014, 1994, 2001, 2016, 1977); WEPA- (1992, 1953, 2005, 1976, 1993) where, for instance, 1977 means the DJFM 1976/1977 winter.

	Computed indices		Climate indices			
	$\max\{R\}$	$\max\{R\}$(land)	R_{WEPA}	R_{NAO}	R_{EA}	R_{SCAND}
Scotland (SC)	0.95	0.95	0.10	**0.89**	0.18	-0.50
Ireland (IR)	0.93	0.90	0.48	**0.79**	0.44	-0.34
Brittany (BR)	0.89	0.89	**0.81**	0.47	.65	-0.10
Biscay (BI)	0.94	0.92	**0.86**	0.45	.57	0.02
Galicia (GA)	0.91	0.90	**0.91**	0.12	.64	0.18
Portugal (PT)	0.92	0.85	**0.80**	-0.22	.58	0.36

Table 1. Correlation coefficient R between the winter-averaged H_s (DJFM) simulated at the 6 buoys (left-hand columns) against simulated optimal ($\max\{R\}$) winter-averaged normalized SLP difference between virtual stations anywhere within the domain (80°-0°W; 0°-70°N) or virtual grid point stations containing land within the corresponding 2.5°x2.5° cell. The right-hand side of the table indicates the correlation coefficient R between the winter-averaged H_s at the 6 buoys and the leading atmospheric modes in the N Atlantic (NAO, EA and SCAND) as well as the WEPA. Bold font indicate the maximum correlation with climate indices.